Near-Infrared Electric Power Generation Through Sub-Energy-Gap Absorption in an Organic–Inorganic Composite

Tsz-Wai Ng, Ming-Fai Lo, Qing-Dan Yang, Man-Keung Fung, and Chun-Sing Lee**

Exploitation of energy from the near-infrared (NIR) region is one strategic approach for enhancing the performance of organic photovoltaic devices (OPVs). While effort has been mostly put toward developing materials with narrow energy gaps, here, a simple approach for harvesting NIR photons with wide-energy-gap materials by making use of their interactive charge-transfer complex (CTC) is shown. It is shown using photoemission studies that the interface between molybdenum (VI) oxide and 5,6,11,12-tetraphenylnaphthacene (MoO_3/rubrene) possesses an abrupt discontinuity in the vacuum level (VL), resulting in significantly overlapped electron wavefunctions and CTC formation. The CTC induces an intermediate state within the original energy gap of rubrene with energy of ≈1.3 eV, suggesting the feasibility of a charge transfer (CT) exciton generated upon NIR excitation. This is confirmed by generation of electric power OPVs with an active layer of MoO_3:rubrene composite under excitation with a NIR light source.

1. Introduction

Organic photovoltaic (OPV) devices based on narrow-energy-gap materials have aroused much attention with strategies to utilize a wider range of photon in the solar spectrum. As commercially available materials (e.g., SnPc, ClAlPc, PbPc) with NIR absorptions are relatively rare, burgeoning interests have been devoted on synthesizing narrow-energy-gap materials with NIR response by creating excited states through excitonic absorption crossing narrow energy gap.[1–5]

Wide bandgap transitional metal oxides with low-lying valence band (VB) levels possesses high electronegativities (i.e. electron affinity energies) have been shown to interact strongly with P-type (or donor) molecules.[6–10] For example, the incorporation of MoO_3 with P-type organic materials such as rubrene, *N,N′*Di(naphthalen-1-yl)-*N,N′*diphenyl-benzidine (NPB), and *N,N′*-diphenyl-*N,N′*-bis(1-naphtylphenyl)-1,1′-biphenyl-4,4′-diamine (α-NPD) results in distinct enhancements in carrier concentrations and film conductivities over those of individual constituents.[6–10] They have been used as connecting units in tandem devices or buffer layer for improving the charge injection in organic light-emitting devices (OLEDs).[10–15] While most works focus on elucidating the mechanisms for charge transport enhancement, these composites also show another profound property of unusual long wavelength absorption band.[6] Previous studies suggest that the absorption in NIR region resides in the formation of a charge-transfer complex (CTC),[6,16] which is a weakly bound electron-hole pair results from electron coupling between the lowest unoccupied molecular orbital (LUMO) of an acceptor molecule with the highest occupied molecular orbital (HOMO) of an donor molecule upon photo-induced electron transfer.[17–21]

However, current knowledge on correlation between NIR absorption and CTC formation is often unclear, especially in transition metal oxide and small-molecule organic materials pairs. Taking MoO_3 and rubrene as an example, **Figure 1** shows a schematic diagram of their reported energy levels, and electron density of state (DOS) in the valence regions.[22,23] It can be seen that the HOMO of rubrene is not overlapping with the conduction band (CB) of MoO_3. The junction formed between MoO_3 and rubrene is behaving as a type III heterojunction with a "broken gap" and should show little interaction. Therefore, the nature of the CT interaction between MoO_3 and rubrene is elusive, and its role on the NIR absorption is ambiguous. Direct insight on CTC formation in MoO_3:rubrene composite and its possibility of charge generation are thus of great interest as the underlying physics will open up new pathway for achieving CTC-based NIR response devices.

While the formation of CTC has been shown to give interesting properties such as NIR absorption, so far there are little report on devices making use of these properties.[24] Herein, we demonstrate generation of electric power upon NIR irradiation on the MoO_3:rubrene composite. By studying the photoluminescence (PL) quenching in the MoO_3:rubrene composite film, we verify the presence of CTC in the MoO_3:rubrene composite. Using ultraviolet and X-ray photoelectron spectroscopies (UPS and XPS) to study the MoO_3/rubrene interface, the origin of NIR absorption and subsequent charge separation process are probed. We conclude that the strong interaction between the two materials induce an intermediate state within the energy gap of rubrene such that direct CT exciton (i.e. the excited electron-hole pair) can be generated through absorbing photons with energies in accordance to the effective energy gap of

Dr. T.-W. Ng, M.-F. Lo, Q.-D. Yang, Dr. M.-K. Fung, Prof. C.- S. Lee
Center of Super-Diamond and Advanced Films (COSDAF)
Department of Physics and Materials Science
City University of Hong Kong
Hong Kong SAR, P. R. China
E-mail: mingflo@cityu.edu.hk; apcslee@cityu.edu.hk

DOI: 10.1002/adfm.201200058

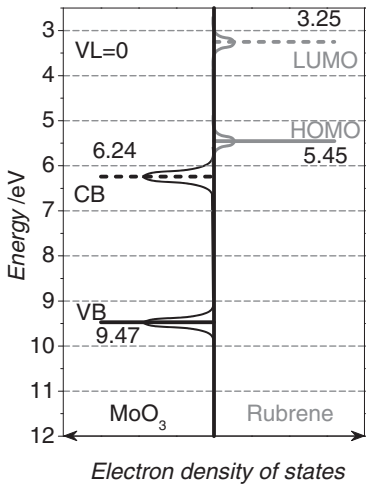

Figure 1. A schematic diagram of energy level alignments of the individual MoO_3 and rubrene under flat band and common VL conditions. The zero energy scale refers to the common VL. The small peaks depict the electron density of states found in the two materials. The HOMO of rubrene does not overlap with the CB of the MoO_3.

~1.3 eV (sub-energy gap absorption in NIR region). Our work shows the feasibility of exploiting the NIR region of the solar spectrum for electric power generation using wide-energy-gap materials.

2. Results and Discussion

2.1. The Existence of a CTC in MoO_3:Rubrene Composites

The absorption properties typically reflect the bandgap energies of semiconducting materials. MoO_3 and rubrene are materials of wide energy gap of ~3.2 and ~2.2 eV respectively. Therefore, both of the materials should not have any NIR response. **Figure 2**a compares the absorption spectra of 35 nm thick films of rubrene, MoO_3 and their composite MoO_3:rubrene (in 1:1 weight ratio) on quartz substrates. The absorption peaks in left panel with photon energies greater than 2.1 eV (<590 nm) correspond to the energy gap absorption of rubrene (2.2 eV). While both MoO_3 and rubrene shows negligible absorption in the right panel (>590 nm), significant absorption features are found in the NIR region below 2 eV in the MoO_3:rubrene composite. This low energy (<2.1 eV) band absorption cannot be attributed to the absorption of either of the individual constituents, but probably the CTC formed between MoO_3 and rubrene.[25–27]

To further probe the existence of CTC in the composite of MoO_3:rubrene, the PL spectra of rubrene and MoO_3:rubrene under different excitation energies are compared. In Figure 2b, 35 nm thick films of single layer rubrene and MoO_3:rubrene are separately deposited on Si-wafers and are excited by 410 nm light. A PL emission at ~620 nm is observed in rubrene (dotted line), which corresponds to exciton state of rubrene. However, this PL emission is totally quenched upon incorporation of MoO_3 (MoO_3:rubrene, solid line). When the same MoO_3:rubrene composite sample is excited at 550 nm (where rubrene absorbs), a new peak emerged at 820 nm (solid line in Figure 2c). Therefore, this 820 nm emission band of the composite should be originated to the excitation of rubrene. The PL results suggest the existence of CT states due to interaction of MoO_3 and rubrene, such that excitons are generated by sub-energy gap photo-excitation as indicated in additional absorption peaks found in the NIR region (i.e., right panel of Figure 2a).

Several recent studies have shown that optical absorption properties of materials can be changed via molecular alignment.[5] To determine whether the newly emerged NIR absorption observed here is result of structural change upon MoO_3 doping, atomic force microscopy (AFM) and X-ray diffraction (XRD) characterizations were carried out. 35 nm thick films of rubrene, MoO_3, and MoO_3:rubrene were prepared on Si wafers and the AFM results are presented in figure S1a to S1c in supporting information. The root-mean-square (RMS) roughness of rubrene, MoO_3 and MoO_3:rubrene composite thin films are 0.58, 0.45, and 0.68 nm, respectively. Line scans of the corresponding regions are also shown (figure S1d to S1f) for better comparison. The peak-to-peak distances are within 2 nm, only limited change is observed after mixing of rubrene and MoO_3. XRD studies were also performed to ascertain changes in structural properties. Similar to the AFM results, no observable difference is found in XRD pattern (not shown here), indicating that the mixed MoO_3: rubrene composite has similar amorphous structure as its constituents.

2.2. Interfacial Dipole-Induced NIR Absorption and Charge-Transfer Characteristics of MoO_3:Rubrene Composite under Ground-State Conditions

The optical results suggest that CTC formed in MoO_3:rubrene composite has been involved in NIR charge generation, but the origin of its occurrence and the involving energy are still unclear. In order to understand the absorption feature and the charge-transfer characteristics in the MoO_3:rubrene composite, the microscopic interfacial electronic and chemical interaction between MoO_3 and rubrene are studied using photoemission analysis.

Figure 3a compares the valence feature measured during rubrene depositions onto a MoO_3 film using UPS (He I). Upon deposition of rubrene on MoO_3, the high binding energy (BE) cutoff region (left panel) abruptly shifts towards the higher BE by 2.04 eV (from curve i to iii). It suggests a decrease of the electrostatic potential of the sample surface and reflects a downwards shift in VL with negative pole directed towards MoO_3.[28–30] Similar VL shift at MoO_3/organic material interface have been previously reported, for example MoO_3/pentacene, MoO_3/CuPc, MoO_3/α-NPD, etc.[31,32] On the right panel of figure 3a, the HOMO (VB) level of rubrene (MoO_3) is determined by taking the spectral onset near the Fermi level (E_f) of the UPS spectra. In curve i, the VB of MoO_3 positioned at 2.60 eV below the E_f. Upon deposition of 0.2 nm of rubrene (nominally one monolayer) on MoO_3 (curve ii), a small HOMO peak emerges with peak edge located at 0.62 eV below the E_f. No further HOMO peak shift is observed when upon further deposition of up to 15 nm rubrene (curve iii).

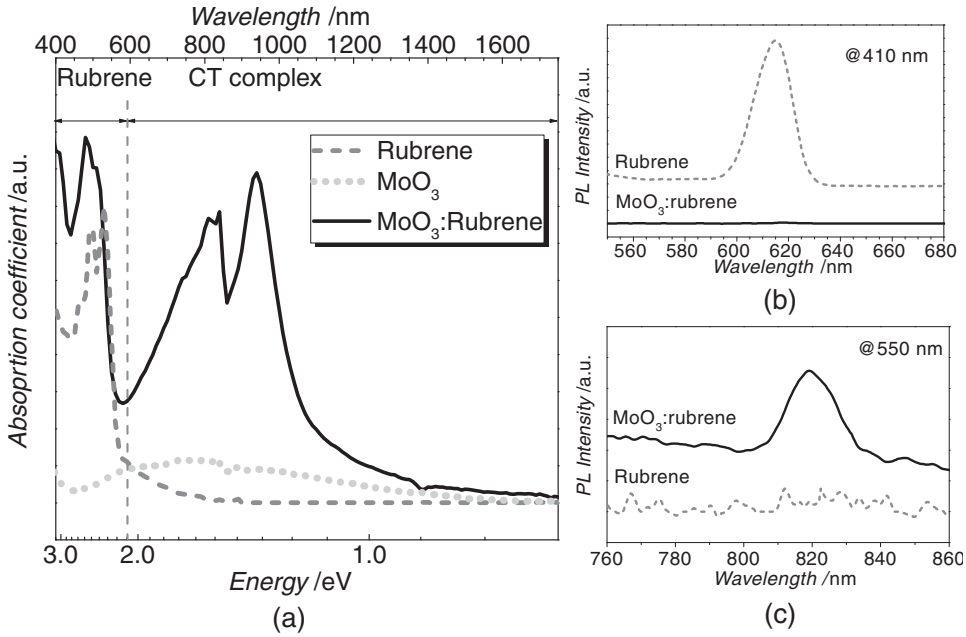

Figure 2. a) UV-Vis-NIR absorption spectra of pristine rubrene (dashed line), pristine MoO_3 (dotted line) and their composite MoO_3:rubrene in 1:1 weight mixing ratio (solid line) prepared on quartz substrates. The strong peak that appears with energy less than 2.1 eV is assigned to the charge-transfer absorption band. b,c) The photoluminescence emission from the rubrene and MoO_3:rubrene composite when excited at b) 410 and c) 550 nm.

This suggests the absence of energy level bending at the interface and thus all VL shift attributes to the presence of an interface dipole. With considerable amount of interfacial states is generated across the junction, significant charge exchange can be accommodated. Therefore, the formation of interface dipole at the junction greatly facilitates electron transfer from rubrene to MoO_3.

A schematic energy level diagram summarizing the UPS results is presented in Figure 3b. The experimentally determined energy level structure of MoO_3/rubrene interface in Figure 3b obviously differs from the expected one in Figure 1 that assuming a common VL. Owing to the strong interfacial dipole formed at MoO_3/rubrene junction at ground-state condition, their interface (Figure 3b) behaves as a "type II" heterojunction (instead of "type III"). More importantly, the resulting staggered gap observed in MoO_3/rubrene interface suggest how photo-excitation leads to sub-energy gap electrons transition from HOMO of rubrene to CB of MoO_3 by gaining energy of about 1.3 eV (i.e., the CTC energy that corresponds to the NIR region of wavelength of ~953 nm).

To further studies the charge-transfer mechanism in the composite, chemical states of Mo in MoO_3:rubrene composite were studied using high-resolution XPS. **Figure 4** depicts the spectra of Mo 3d core levels for pristine MoO_3 (curve i) and MoO_3:rubrene composite (curve ii) prepared on ITO substrates. The Mo 3d with spin orbital splitting were fitted according to Mo $3d_{5/2}$ and $3d_{3/2}$ using Gaussian function. In a pure MoO_3 film (curve i), the fitted Mo peaks with BE values of 232.5 ($3d_{5/2}$) and 235.77 eV ($3d_{3/2}$) can be assigned to oxidation state of 6+.[33–35] It is noted that the spectrum of MoO_3:rubrene composite (curve ii) shows an additional shoulder components with peak position located at lower BE at 231.7 ($3d_{5/2}$) and 234.7 eV ($3d_{3/2}$), which refer to oxidation state of 5+.[35] The reduction of Mo 6+ cations to states of Mo 5+ after incorporation of rubrene ($C_{42}H_{28}$) indicates either an electron gain from rubrene or the bond formation of Mo-C. Either phenomenon provides an electric field for the electron transfer from MoO_3 to rubrene in the composite at ground-state condition, where it facilitates CT exciton dissociation.

The results from PL studies suggest the existence of CTC state in MoO_3:rubrene composite material in NIR region. Due to the large interfacial dipole at the MoO_3/rubrene interface as observed in UPS results, it is ascertained that an intermediate CT state is induced in the sub-energy gap of rubrene such that photon absorption takes place with energy in accordance of the effective energy gap of the composite, i.e., ~1.3 eV (in NIR region). The bounded CT excitons are photogenerated by exciting electron from the HOMO rubrene to the CB of MoO_3.[6] The exciton would subsequently be dissociated by the strong interactive charge-transfer interface within the composite in ground-state condition, where electrons are spontaneously transferred from rubrene to MoO_3 via reducing the oxidation state of Mo from 6+ to 5+. Thus, the strongly interacting MoO_3/rubrene bulk heterojunction in the composite is the core of the charge generation process.

2.3. The Involvement of MoO_3:Rubrene CTC in Electric Power Generation

To verify whether charge separation takes place in the MoO_3:rubrene composite, different devices were fabricated.

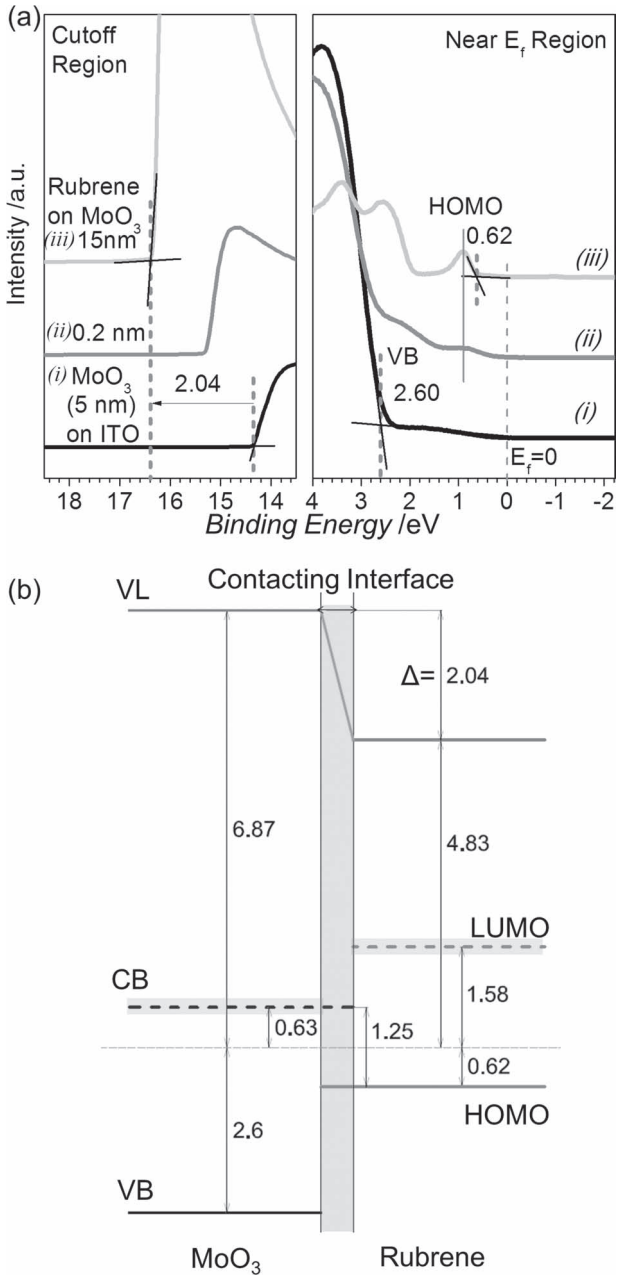

Figure 3. a) Evolution of UPS (He I) spectra showing the valence features of i) 5 nm MoO_3 on ITO substrate, ii) 0.2 nm rubrene and iii) 15 nm rubrene on MoO_3/ITO substrate at both secondary cutoff and near Fermi level regions. The dotted lines are marked for recognizing energy shifts of spectral onsets. b) Energy level diagram of MoO_3/rubrene interface. Values of the HOMOs are deduced from the onset position of the HOMO peaks in (a), while the LUMO of the rubrene is determined by considering the optical bandgap. The CB of MoO_3 is estimated from the charge-transport gap reported previously. All values are given in eV.

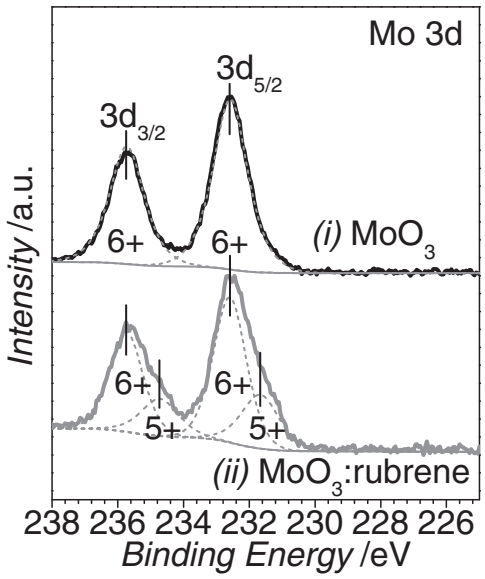

Figure 4. XPS spectra of the Mo 3d core levels for i) pristine MoO_3 films and ii) MoO_3:rubrene composite deposited on ITO substrates. The dotted line shows the peak deconvolution based on a Gaussian function.

Figure 5a,b depicts the normalized short-circuit photocurrent (J_{sc}) and open-circuit photovoltage (V_{oc}) of the devices with different configurations characterized under illumination of 870 nm LED with increasing light intensities from 0 to 300 mW/cm^2. Even though the MoO_3:rubrene composite shows NIR absorption, device a with this single composite active layer (□: ITO/MoO_3:rubrene (35 nm)/bathocuproine BCP (7 nm)/Al) shows no photoresponse.

One possible reason for the lack of NIR response might be the subsequent nonradiative decay in the composite layer. To verify this, we modify the device by adding a layer of high electron-drawing and electron-transporting fullerene (C_{60}) adjacent to the active composite, device b (■: ITO/MoO_3:rubrene (35 nm)/C_{60} (40 nm)/BCP (7 nm)/Al). Interestingly, the photocurrent of device b increases linearly with the illumination intensity. The device generates ~0.15V photovoltage at illumination intensity of 300 Wm^{-2}. To determine the role of C_{60}, photoresponse of bilayer device c (Δ: ITO/rubrene (35 nm)/C_{60} (40 nm)/BCP (7 nm)/Al) and device d (○: ITO/MoO_3 (35 nm)/C_{60} (40 nm)/BCP (7 nm)/Al) are included. The absence of photoresponse in bilayer devices c and d confirms that charge separation is not attributed to the interfacial charge interaction with adjacent C_{60} (i.e. rubrene/C_{60} or MoO_3/C_{60}).

To further consolidate our discussion on the NIR response, all devices are characterized using a light source with wide NIR waveband under dark and under illumination of 150 W solar simulator equipped with a FSG-RG 850 and 1000 nm colored glass filters which block light with wavelength below 850 and 1000 nm respectively. For reference, the transmission spectra of the FSG-RG 850 and 1000 nm colored filters were shown in Figure 5c. The NIR irradiation intensity is controlled at 50 mW/cm^2. The current density-voltage (J-V) responses for all the devices are shown in Figure 5d–f.

Figure 5d depicts the J-V characteristics of the device a. Upon NIR illumination, the photocurrent of device a, which consists of a single MoO_3:rubrene composite layer has increased from ~40 mA/cm^2 (in dark condition) to ~60 mA/cm^2 under an applied bias voltage of −1.4 V. However, it is noted that in the absence of external bias voltage, the device shows zero Jsc and

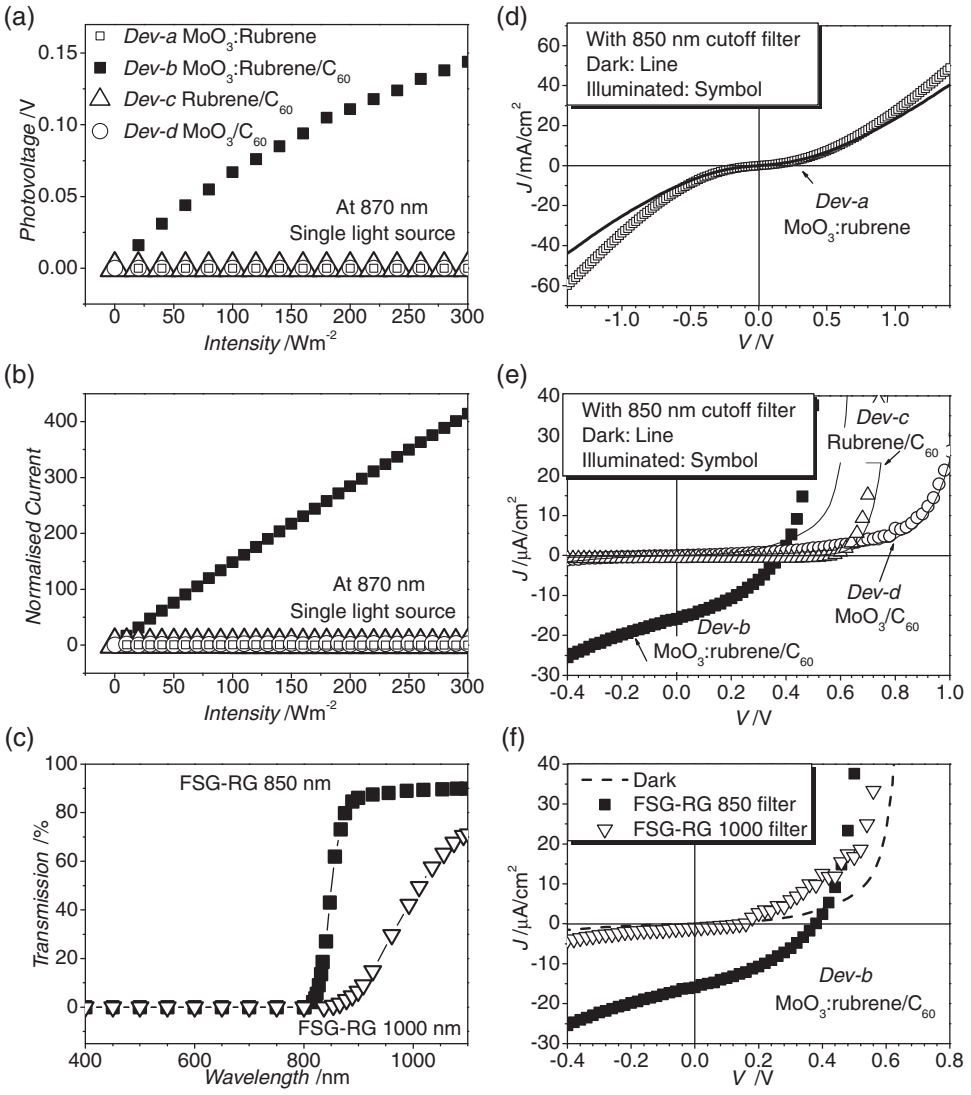

Figure 5. Photoresponse of NIR OPV devices in term of a) photocurrent and b) photovoltage when under a NIR illumination using 870 nm LED light source of increasing intensities. The device configurations are also shown. c) The transmission spectra of the filters used. d) Current density-voltage (J-V) characteristics of device a (□) under 50 mW cm^{-2} irradiation with a solar simulator equipped with the FSG-RG 850 nm cutoff filter. e) J-V characteristics of device b (■), device c (Δ) and device d (○) under the same condition. f) J-V characteristics of device b measured using either a 850 (■) or 1000 (▽) nm high-pass filter. Dark J-V characteristics are shown as lines without symbols.

Voc under NIR illumination, suggesting that no photocurrent can be obtained without the assistant of an external bias voltage. Interestingly when C_{60} is added in adjacent to the MoO_3:rubrene composite (i.e. device b with MoO_3:rubrene/C_{60}), PV response is observed with a Voc of 0.38 V, Jsc of 15.9 μA/cm^2 and fill factor (FF) of 0.36 as shown in Figure 5e. To confine whether the observed photoresponse is originated from the CTC absorption peak observed in Figure 2a, the device is characterized again using a FSG-RG 1000 filter and the result is illustrated as in Figure 5f. (The log J-V characteristics of the "device b" under dark and illumination with FSG-RG 850 and FSG-RG 1000 filter are shown in Figure S2 in Supporting Information.) As only limited Jsc is observed (< 1 μA/cm^2) in "device b" when FSG-RG 1000 filter is used, it suggests that most of the J–V responses observed in Figure 5f originate from NIR waveband between 850 to 1000 nm.

These PV responses of device a and device b suggest that the NIR photo-induced charge separation does take place within the composite layer. The charge separation in the MoO_3:rubrene composite would in-turn satisfactorily explain the PL quenching as shown in Figure 2b. To understand the NIR response of device b (i.e., the MoO_3:rubrene/C_{60}), it is important to recall the factor that limiting the photovoltaic parameters such as V_{oc} and J_{sc}. The CTC with energy quantified as the energy difference between the HOMO of donor and LUMO of acceptor (i.e., 1.3 eV for MoO_3:rubrene composite) contribute to charge separation by providing a stable state that assists the separation and recombination of the charge pairs in the blend film. While

the energy of the CTC primarily sets the upper limit for the V_{oc},[36–40] it also critically determines whether photocurrent is generated, or energy transfer and subsequent emission from the constituent singlet state.[26] Furthermore, the NIR response is originated from CTC state formed under the ground state interaction inside the MoO_3:rubrene composite, limited exciton lifetime is expected due to exciton-phonon-induced recombination, i.e., internal conversion.[5,41]

By using appropriate dopant, we successfully demonstrate a NIR device using wide band gap material. Although only limited photocurrent is observed at this stage, a sufficiently large Voc is observed upon light illumination of single 870 nm (0.15 V) and wide NIR waveband (0.38 V). Furthermore, a linear increase in photogenerated current to 400 times of initial value is observed at zero bias when NIR light intensity increased from 10 to 300 W m^{-2}, suggesting other possible applications such as sensor and detector.[24]

2.4. The Role of the Adjacent C_{60} Layer on Charge Extraction from MoO_3:Rubrene Composites

Another interesting phenomenon observed is the NIR photoresponse of the MoO_3:rubrene composite when a C_{60} layer is insert between the composite and BCP layer. To probe the role of C_{60} and examine how it facilitates charge extraction, the electronic structures of MoO_3:rubrene/C_{60} interface is investigated using UPS. **Figure 6**a shows UPS spectra of the MoO_3:rubrene/C_{60} interface in secondary electron cutoff (left) and the near E_f (right) regions. The bottom spectrum corresponds to the spectrum from a 10 nm MoO_3:rubrene composite film prepared on ITO substrate. The high BE cutoff is located at 16.15 eV (left panel). A small peak that refers as the "effective HOMO" of the composite has spectral onset position of 0.24 eV (right panel). Therefore, the VL and the effective HOMO level of the MoO_3:rubrene composite are located at 5.02 and 0.24 eV respectively as shown in Figure 6b.

Upon deposition of C_{60}, the effective HOMO peak in the underlying MoO_3:rubrene composite shows negligible energy shift. Meanwhile, both electron cutoff and the HOMO of C_{60} slightly shift towards the lower BE by 0.2 eV at the interface, suggesting no interfacial dipole is involved at the MoO_3:rubrene/C_{60} junction.

The energy levels of C_{60} are all upwards shifted by ~0.2 eV during the initial deposition of 0.8 nm C_{60} (Figure 6b). The resultant internal E-field at MoO_3:rubrene/C_{60} junction assists the electrons transfer and facilitates the charge extraction from the MoO_3:rubrene composite to C_{60} under the ground-state condition, thus minimizes electron-hole recombination in the composite layer. With reduced nonradiative recombination, the open circuit voltage is observed for device b with (MoO_3:rubrene/C_{60}).[40] It is also noted that the LUMO of C_{60} lies slightly below the effective LUMO of the MoO_3:rubrene composite. Therefore, the C_{60} layer adjacent to the MoO_3:rubrene composite provides a barrier-free electron transport across the interface; meanwhile its low-lying HOMO levels act as an effective barrier for hole blocking. This explains why device b (■: MoO_3:rubrene/C_{60}) exhibits a photovoltaic effect with an addition layer of C_{60} upon NIR light illumination.

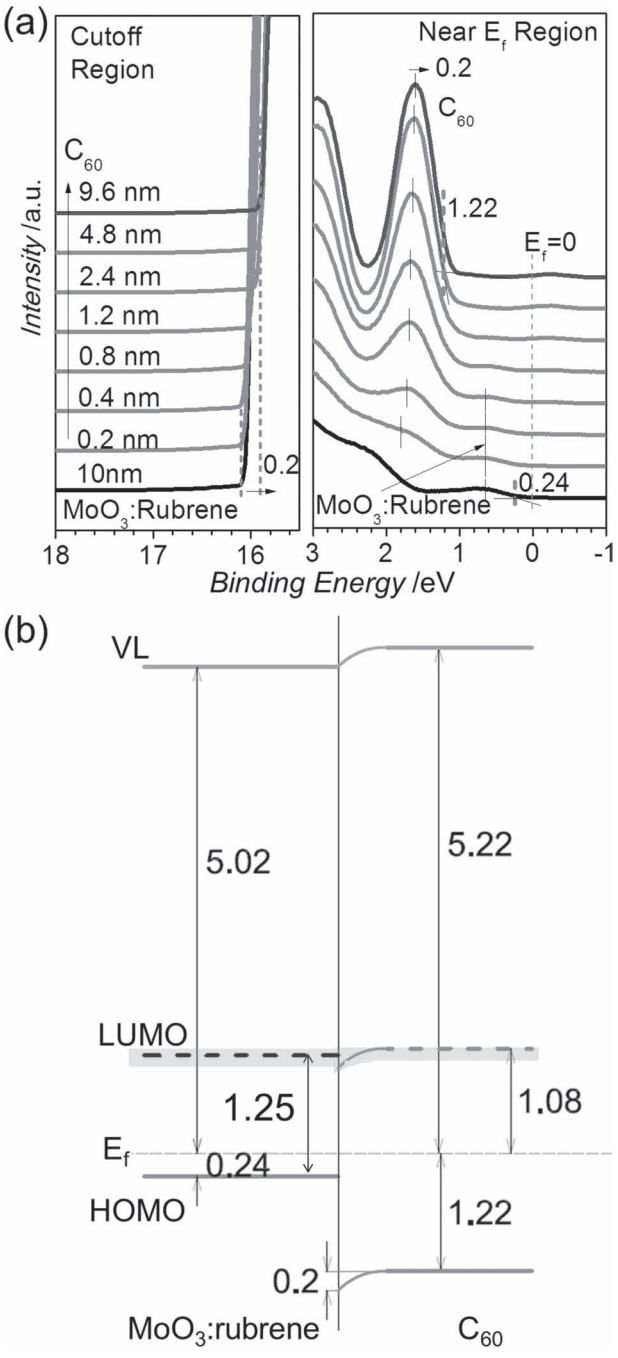

Figure 6. a) Evolution of UPS (He I) spectra showing the valence features of a C_{60}/10 nm MoO_3:rubrene composite with increasing function of C_{60} thickness at both secondary cutoff and near Fermi level regions. The dotted lines are marked for recognizing energy shifts of spectral onsets. b) Energy level diagram of MoO_3:rubrene/C_{60} interface. Values for the HOMOs are deduced from the onset position of the HOMO peaks in (a). The LUMO of the MoO_3:rubrene composite is extracted from the effective band gap, i.e., 1.25 eV, in Figure 4b; and the LUMO of C_{60} is estimated from the previously reported bandgap.[42] All values are given in eV.

In contrast with the previous reported NIR photocharge generation which photon energy absorption made by exciting electron crossing the energy gap of a single material, the CTC-induced charge generation process involves: 1) photon

absorption with energy in accordance of the "effective bandgap" of the functional composite, i.e. the sub-bandgap absorption through an intermediate states in the forbidden gap of the organic material; 2) creation of a bounded CT exciton by exciting electron across the effective energy gap of the composite, i.e., from HOMO of rubrene to the CB of MoO_3; and 3) subsequent splitting of these excitons by the strongly interactive charge transfer interfaces within the composite in ground-state condition. Therefore, the strongly interactive MoO_3/rubrene interface in the composite is the core of the whole charge generation and dissociation processes.

3. Conclusions

The NIR electric power generation process using MoO_3:rubrene composite are successfully demonstrated. With studies of PL quenching and valence band features, we find that the CTC formed due a discontinuity in the VL. This interfacial dipole induces an intermediate state within the energy gap of rubrene. CT exciton thus can be generated by electron transition from the HOMO of rubrene to the CB of MoO_3 upon photon absorption with energy in accordance to the effective energy gap of the MoO_3:rubrene composite at ~1.3 eV in NIR region. With strong electron coupling in ground-state condition, the formed electron-hole pair will be readily separated via reducing the oxidation state of Mo from 6+ to 5+. The whole process of NIR power generation is attributed to the charge-transfer process in the functional composite. This finding may open up new research windows for NIR charge generation based on CTC formed between wide-energy-gap materials.

4. Experimental Section

All devices were prepared on patterned indium-doped tin oxide (ITO) coated glasses, which were cleaned using ethanol, followed by Decon 90 and de-ionized water. Then, the substrates were UV-ozone treated for 15 minutes. The substrates were transfer into an evaporation chamber with a base pressure of ~ 10^{-7} Torr. Organic films were thermally deposited on the ITO substrate from crucibles. All active materials including MoO_3, rubrene, C_{60} and BCP (all from Luminescence Technology Corp.) were used as received. The deposition rate with rates controlled by a quartz oscillating thickness monitor at 0.1-0.2 nm/s. The MoO_3:rubrene composite film are prepared by co-evaporating MoO_3 and rubrene at a controlled weight ratio of 1:1. No intentional temperature treatment was used during nor after device fabrication. The active devices areas were defined by the overlapped region of the ITO layer and the Al layer at ~0.12 cm^2. The OPV devices were fabricated with following configurations: device a: ITO/MoO_3:rubrene (35 nm)/BCP (7 nm)/Al (80 nm); device b: ITO/MoO_3:rubrene (35 nm, 1:1 weight ratio)/C_{60} (40 nm)/BCP (7 nm)/Al (80 nm); device c: ITO/rubrene (35 nm)/C_{60} (40 nm)/BCP (7 nm)/Al (80 nm); and device d: ITO/MoO_3 (35 nm)/C_{60} (40 nm)/BCP (7nm)/Al (80nm). The completed devices were then transferred to a nitrogen-filled glove box and encapsulated using glass caps and UV curing epoxy resin.

The photocurrent and photovoltage were characterized using Zahner IM 6 electrochemical workstation equipped with controlled intensity modulated photo-spectroscopy (CIMPS). A calibrated NIR light-emitting diode (LED) light source with illumination wavelength at 870 nm is used for all devices measurements. To characterize the photovoltaic response over a wide NIR range, the composite device was also measured with a programmable Keithley model 237 power source in the dark and under 50mW/cm^2 illumination. To examine the NIR photovoltaic response, the device is illuminated under a 150 W solar simulator equipped with the FSG-RG 850 and 1000 nm cutoff colored glass filters (the transmission spectrum of the filters are shown in Figure 5c). Therefore, the visible region of the solar simulator is filtered, and all the photovoltaic response corresponds to remaining NIR-to-IR region.

All photoemission studies were carried out using a VG ESCALAB 220i-XL surface analysis system equipped with a He-discharge lamp providing He-I photons of 21.22 eV for UPS analysis; and a monochromatic Al-Kα X-ray gun with photons energies of 1486.6 eV for XPS investigation. The base vacuum of the system is 10^{-10} Torr. ITO-coated glass substrates were thoroughly cleaned before loading into the ultrahigh vacuum (UHV). MoO_3, rubrene and MoO_3:rubrene are stepwisely deposited by thermal evaporation inside the deposition chamber at a pressure of ~2×10^{-9} Torr. Freshly prepared sample was in situ transferred to the another chamber for UPS and XPS measurements without vacuum break. All XPS measurements were calibrated with reference to the freshly sputtered Au $4f_{7/2}$ core level (83.98 eV). The absolute energy resolution of the analyzer was set as 0.018 eV for the UPS measurement so that the spectral resolution was 0.09 eV as estimated from the Fermi edge of Au. UPS He I measurements were performed to study the valence states of the prepared films. VL offsets were obtained from the shifts of the intensity thresholds at the lowest inelastic electrons kinetic energy cut-off, with a bias of -5.0 V with respect to ground. All spectra presented were plotted with respect to the determined E_f. The energy gaps of the MoO_3 were estimated by considering the charge-transfer energy gap reported from inversed photoemission spectroscopy (IPES) from previous studies, i.e., 3.23 eV.[22] All experimental details have been previously reported.[42,43]

Supporting Information

Supporting Information is available from the Wiley Online Library or from the author.

Acknowledgements

The work described in this paper was supported by a grant from the Research Grants Council of the Hong Kong Special Administrative Region, China (Project No. T23-713/11).

Received: January 9, 2012
Revised: February 14, 2012
Published online: April 13, 2012

[1] R. F. Bailey-Salzman, B. P. Rand, S. R. Forrest, *Appl. Phys. Lett.* **2007**, *91*, 013508.
[2] B. P. Rand, J. Xue, F. Yang, S. R. Forrest, *Appl. Phys. Lett.* **2005**, *87*, 233508.
[3] D. Y. Kim, G. Sarasqueta, F. So, *Sol. Energy Mater. Sol. Cells* **2009**, *93*, 1452.
[4] M. Hiramoto, K. Kitada, K. Iketaki, T. Kaji, *Appl. Phys. Lett.* **2011**, *98*, 023302.
[5] J. D. Zimmerman, V. V. Diev, K. Hanson, R. R. Lunt, E. K. Yu, M. E. Thompson, S. R. Forrest, *Adv. Mater.* **2010**, *22*, 2780.
[6] T. Matsushima, G. H. Jin, Y. Kanai, T. Yokota, S. Kitada, T. Kishi, H. Murata, *Org. Electron.* **2011**, *12*, 520.
[7] M. Kubo, K. Iketaki, T. Kaji, M. Hiramoto, *Appl. Phys. Lett.* **2011**, *98*, 073311.
[8] H. Nakanotani, H. Kakizoe, C. Adachi, *Solid State Commun.* **2011**, *151*, 93.
[9] X. Qiao, J. Chen, X. Li, D. Ma, *J. Appl. Phys.* **2010**, *107*, 104505.
[10] W. J. Shin, J. Y. Lee, J. C. Kim, T. J. Yoon, T. S. Kim, O. K. Song, *Org. Electron.* **2008**, *9*, 333.

[11] J. P. Yang, Y. Xiao, Y. H. Deng, S. Duhm, N. Ueno, S. T. Lee, Y. Q. Li, J. X. Tang, *Adv. Funct. Mater.* **2012**, *22*, 600.
[12] J. Qin, Z. B. Wang, M. G. Helander, Z. H. Lu, *Appl. Phys. Lett.* **2011**, *99*, 153305.
[13] Q. Y. Bao, J. P. Yang, Y. Q. Li, J. X. Tang, *Appl. Phys. Lett.* **2010**, *97*, 063303.
[14] J. X. Tang, M. K. Fung, C. S. Lee, S. T. Lee, *J. Mater. Chem.* **2010**, *20*, 2539.
[15] M. Zhang, H. Wang, H. Tian, Y. Geng, C. W. Tang, *Adv. Mater.* **2011**, *23*, 4960.
[16] E. D. Głowacki, K. L. Marshall, C. W. Tang, N. S. Sariciftci, *Appl. Phys. Lett.* **2011**, *99*, 043305.
[17] L. Goris, K. Haenen, M. Nesladek, P. Wagner, D. Vanderzande, L. De Schepper, J. De Schepper, J. D'Haen, L. Lusten, J. V. Manca, *J. Mater. Sci.* **2005**, *40*, 1413.
[18] L. Goris, A. Poruba, L. Hod'akova, M. Vanecek, K. Haenen, M. Nesladek, P. Wagner, D. Vanderzande, L. De Schepper, J. V. Manca, *Appl. Phys. Lett.* **2006**, *88*, 052113.
[19] D. Veldman, S. C. J. Meskers, R. A. J. Janssen, *Adv. Funct. Mater.* **2009**, *19*, 1939.
[20] S. R. Forrest, *Chem. Soc. Rev.* **1997**, *97*, 1793.
[21] M. Riede, T. Mueller, W. Tress, R. Schueppel, K. Leo, *Nanotechnology* **2008**, *19*, 424001.
[22] Irfan, M. Zhang, H. Ding, C. W. Tang, Y. Gao, *Org. Electron.* **2011**, *12*, 1588.
[23] H. Ding, Y. Gao, *Appl. Phys. A* **2009**, *95*, 89.
[24] S. H. Wu, M. F. Lo, Z. Y. Chen, T. W. Ng, H. W. Mo, X. Hu, C. Wu, W. L. Li, C. S. Lee, *Phys. Status Solidi* **2011**, *6*, 129.
[25] R. Foster, *Organic Charge-Transfer Complexes*, Academic Press, New York **1969**.
[26] J. J. Benson-Smith, L. Goris, K. Vandewal, Ken Haenen, J. V. Manca, D. Vanderzande, D. D. C. Bradley, J. Nelson, *Adv. Funct. Mater.* **2007**, *17*, 451.
[27] K. Vandewal, A. Gadisa, W. D. Oosterbaan, S. Bertho, F. Banishoeib, I. V. Severen, L. Lutsen, T. J. Cleij, D. Vanderzande, J. V. Manca, *Adv. Funct. Mater.* **2008**, *18*, 2064.
[28] H. Ishii, K. Sugiyama, E. Ito, K. Seki, *Adv. Mater.* **1999**, *11*, 605.
[29] H. Ishii, K. Seki, *IEEE Trans. Electron Devices* **1997**, *44*, 1295.
[30] D. Cahen, A. Kahn, *Adv. Mater.* **2003**, *15*, 271.
[31] H. Wang, Z. Liu, M. F. Lo, T. W. Ng, C. S. Lee, D. Yan, S. T. Lee, *J. Appl. Phys.* **2010**, *107*, 024540.
[32] M. Kröger, S. Hamwi, J. Meyer, T. Riedl, W. Kowalsky, A. Kahn, *Appl. Phys. Lett.* **2009**, *95*, 123301.
[33] T. H. Fleisch, G. J. Mains, *J. Chem. Phys.* **1982**, *76*, 780.
[34] R. J. Colton, A. M. Guzman, J. W. Rabalais, *J. Appl. Phys.* **1978**, *49*, 409.
[35] M. Zhang, Irfan, H. Ding, Y. Gao, C. W. Tang, *Appl. Phys. Lett.* **2010**, *96*, 183301.
[36] M. C. Scharber, D. Mühlbacher, M. Koppe, P. Denk, C. Waldauf, A. J. Heeger, C. J. Brabec, *Adv. Mater.* **2006**, *18*, 789.
[37] B. P. Rand, D. P. Burk, S. R. Forrest, *Phys. Rev. B* **2007**, *75*, 115327.
[38] M. F. Lo, T. W. Ng, T. Z. Liu, V. A. L. Roy, S. L. Lai, M. K. Fung, C. S. Lee, S. T. Lee, *Appl. Phys. Lett.* **2010**, *96*, 113303.
[39] K. Vandewal, K. Tvingstedt, A. Gadisa, O. Inganäs, J. V. Manca, *Nat. Mater.* **2009**, *8*, 904.
[40] C. Deibel, T. Strobel, V. Dyakonov, *Adv. Mater.* **2010**, *22*, 4097.
[41] H. S. Cho, D. H. Jeong, S. Cho, D. Kim, Y. Matsuzaki, K. Tanaka, A. Tsuda, A. Osuka, *J. Am. Chem. Soc.* **2002**, *124*, 14642.
[42] T. W. Ng, M. F. Lo, M. K. Fung, S. L. Lai, Z. T. Liu, C. S. Lee, S. T. Lee, *Appl. Phys. Lett.* **2009**, *95*, 203303.
[43] M. F. Lo, T. W. Ng, S. L. Lai, F. L. Wong, M. K. Fung, S. T. Lee, C. S. Lee, *Appl. Phys. Lett.* **2010**, *97*, 143304.